International Journal of Heat and Mass Transfer 52 (2009) 4040–4046

Contents lists available at ScienceDirect

International Journal of Heat and Mass Transfer

journal homepage: www.elsevier.com/locate/ijhmt

# Numerical simulation of laminar breakdown and subsequent intermittent and turbulent flow in parallel-plate channels: Effects of inlet velocity profile and turbulence intensity

W.J. Minkowycz [a,*], J.P. Abraham [b], E.M. Sparrow [c]

[a] University of Illinois at Chicago, Department of Mechanical and Industrial Engineering, Chicago, IL 60607, USA
[b] Laboratory for Heat Transfer and Fluid Flow Practice, School of Engineering, University of St. Thomas, St. Paul, MN 55105-1079, USA
[c] Laboratory for Heat Transfer and Fluid Flow Practice, Department of Mechanical Engineering, University of Minnesota, Minneapolis, MN 55455-0111, USA

ARTICLE INFO

*Article history:*
Received 18 November 2008
Accepted 23 March 2009
Available online 8 May 2009

*Keywords:*
Parallel-plate channel
Laminar-turbulent transition
Fully developed intermittency
Transition Reynolds number
Inlet velocity profile
Inlet turbulence intensity

ABSTRACT

The nature of flow development in a parallel plate channel has been investigated by making use of a newly developed model of intermittency. That model, taken together with the RANS equations of momentum conservation, the continuity equation, and the SST turbulence model, was employed to provide a complete chronology of the development processes and the derived practical results. A major focus of the work is the effect of inlet conditions on the downstream behavior of the developing flow. It was observed that the flow development process depends critically on the specifics of the inlet conditions characterized here by the shape of the velocity profile and the magnitude of the turbulence intensity. Two velocity profile shapes (flat and parabolic), are regarded as limiting cases. Similarly, two turbulence intensities, $Tu$ = 1% and 5%, are employed. From the standpoint of practice, the relationship between the friction factor and the Reynolds number is most significant. It was found that this relationship reflects that of standard practice for only one of the investigated cases (flat velocity profile, $Tu$ = 5%). For the other cases (flat profile, $Tu$ = 1% and parabolic profile, $Tu$ = 1% and 5%), the breakdown of laminar flow is delayed and the onset of full turbulence occurs rather abruptly at $Re \sim$10,000. Three unique fully developed flow regimes are existent, depending on the inlet conditions and on the value of the Reynolds number. In addition to the standard laminar and fully turbulent regimes, another regime, *fully developed intermittent*, can occur. Specifically, in the latter regime, laminar and turbulent flows occur intermittently.



## 1. Introduction

Although flow in large-aspect-ratio rectangular ducts may be considered a mature area of fluid flow research, a careful appraisal reveals the contrary. For example, the considerable ambiguity in the nature of the fluid flow at the duct inlet has a significant effect on its downstream behavior [1]. In fact, a careful assessment of the relevant literature indicates that aside from [2], only qualitative descriptions of the inlet conditions are given. As a second illustration of the uncertainties associated with the available information about flow in flat rectangular channels, it has been pointed out in [3] that the hydraulic diameter is not the optimal characteristic dimension in the Reynolds number and friction factor.

In the present research, a non-empirical, quantitative approach is taken to the fluid flow in a parallel-plate channel, which is the limit of large-aspect-ratio ducts. The objective of the present work is to numerically simulate and predict the breakdown of laminar flow, the ensuing intermittent flow, and the attainment of a fully developed regime which may be either intermittent or fully turbulent. The dependency of these outcomes on the nature of the flow field at the duct inlet will be explored by varying the turbulence intensity and the shape of the velocity profile. Other characteristics that will be explored include the locations of laminar breakdown and the attainment of fully developed flow.

The literature on fluid flow in flat rectangular ducts and parallel-plate channels can be classified into three categories. One of these encompasses papers in which empirical information is given on the friction factor and its dependence on the Reynolds number [2–11]. Some of these papers used the height of the duct as the characteristic dimension whereas others utilized the hydraulic diameter. In [3], which is a retrospective view of an accumulation of data, it was suggested that the optimal characteristic dimension is 2/3 of the traditional hydraulic diameter. In many of the cited references, no mention was made of the conditions at the duct inlet. In those cases where a qualitative description was given, the sharp-edged inlet was used. The exception is that of [2]. There, a careful control of the turbulence intensity was achieved by the

* Corresponding author. Tel.: +1 312 996 3467; fax: +1 312 413 0447.
*E-mail address:* wjm@uic.edu (W.J. Minkowycz).

0017-9310/$ - see front matter © 2009 Elsevier Ltd. All rights reserved.
doi:10.1016/j.ijheatmasstransfer.2009.03.041

**Nomenclature**

| | |
|---|---|
| $A$ | transitional model constant |
| $E$ | model destruction terms |
| $H$ | channel height |
| $F_1$, $F_2$ | blending functions in SST model |
| $p$ | pressure |
| $P$ | model production term |
| $Re$ | Reynolds number based on hydraulic diameter and average velocity |
| $S$ | absolute value of the shear strain rate |
| $Tu$ | turbulence intensity |
| $u$ | $x$ velocity |
| $U$ | average velocity |
| $\upsilon$ | $y$ velocity |
| $x,y$ | coordinate directions |

*Greek symbols*

| | |
|---|---|
| $\beta_1$, $\beta_2$ | SST model constants |
| $\omega$ | specific rate of turbulence dissipation |
| $\mu$ | dynamic viscosity |
| $\kappa$ | turbulent kinetic energy |
| $\Pi$ | intermittency adjunct function |
| $\gamma$ | intermittency |
| $\rho$ | density |
| $\sigma$ | Prandtl number |

*Subscripts*

| | |
|---|---|
| *turb* | turbulent |

use of screens, a honeycomb, and a contraction ratio of 24:1 upstream of the duct. The contraction also compresses the boundary layers, so that it may be expected that the velocity profile at the duct inlet was relatively flat with high velocity gradients adjacent to the bounding walls. Notwithstanding the aforementioned uncertainties, a general consensus of the results of [2–11] is that laminar breakdown in flat rectangular ducts occurs for a Reynolds number on the order of 2500–4000, where the Reynolds number is based on the mean velocity and the hydraulic diameter.

The second category into which work on laminar breakdown can be placed is highly mathematical and deals with the response of the parabolic velocity profile to various types of disturbances [12–17]. Noteworthy is the result that for two-dimensional disturbances, the breakdown of laminar flow was found to occur at $Re \sim 15{,}000$. This seemingly high Reynolds number reflects the fact that no account has been taken of the nature of the flow at the inlet of the duct and that a pre-existing parabolic profile was the starting point to which disturbances were applied.

In the third category are experimental works whose focus is the verification and elucidation of the stability theory [18–20]. In all of these works, artificial disturbances were introduced, either by an electromagnetic solenoid or by a vibrating ribbon. The outcomes of these experiments were inconsistent in that for [19–20], the critical Reynolds number was below that of linear stability theory, whereas in [18], the breakdown occurred at Reynolds numbers consistent with stability theory.

In a recent publication [21], the authors have dealt with a companion problem to that being considered here, namely, the fluid flow in a round pipe which undergoes transitions from laminar-to-intermittent transitional flow and from transitional flow to either fully developed intermittent or fully developed turbulent flow.

## 2. Simulation model

The geometry of the model is two-dimensional with a symmetry plane extending along the half-height of the channel. The velocity at the inlet will be prescribed along with the turbulence intensity. Two limiting velocity profiles will be employed. One of these is a uniform profile which is intended to represent the limiting profile for a fully developed turbulent flow. The second profile is the parabolic distribution which corresponds to a fully developed laminar flow. It is believed that these two limits are sufficient to reveal the trend-wise dependence of the downstream physical processes on the shape of the inlet velocity profile. In addition, the turbulence intensity was varied over the range from 1% (low) to 5% (high).

### 2.1. Governing equations

To implement the goals of this study, use has been made of a transition model devised by Menter and co-workers [22–24]. That model, when used in conjunction with the shear stress transport (SST) turbulence model, provides a complete picture encompassing all unidirectional flow regimes. The Menter model was designed to deal with external flows; it was modified in [21] to be applicable to internal flows. Its validity for such use was verified by comparison with both experimental data and with empirical correlations. That verification has encouraged its application here.

The total description of the model involves a set of seven partial differential equations for a two-dimensional flow. The first of these represents conservation of mass, while the second and third are the Reynolds-averaged Navier–Stokes equations.

$$\frac{\partial u_i}{\partial x_i} = 0 \tag{1}$$

$$\rho\left(\frac{\partial(u^2)}{\partial x}+\frac{\partial(u\upsilon)}{\partial y}\right) = -\frac{\partial p}{\partial x}+\frac{\partial}{\partial x}\left((\mu+\mu_{turb})\frac{\partial u}{\partial x}\right) + \frac{\partial}{\partial y}\left((\mu+\mu_{turb})\frac{\partial u}{\partial y}\right) \tag{2}$$

and

$$\rho\left(\frac{\partial(u\upsilon)}{\partial x}+\frac{\partial(\upsilon^2)}{\partial y}\right) = -\frac{\partial p}{\partial y}+\frac{\partial}{\partial x}\left((\mu+\mu_{turb})\frac{\partial \upsilon}{\partial x}\right) + \frac{\partial}{\partial y}\left((\mu+\mu_{turb})\frac{\partial \upsilon}{\partial y}\right) \tag{3}$$

The next pair of equations represents the SST turbulence model which has been modified to accommodate the intermittency $\gamma$. The intermittency is the multiplier of the turbulent production term $P_\kappa$.

$$\frac{\partial(\rho u\kappa)}{\partial x}+\frac{\partial(\rho\upsilon\kappa)}{\partial y} = \gamma\cdot P_\kappa - \beta_1\rho\kappa\omega + \frac{\partial}{\partial x}\left[\left(\mu+\frac{\mu_{turb}}{\sigma_\kappa}\right)\frac{\partial\kappa}{\partial x}\right] + \frac{\partial}{\partial y}\left[\left(\mu+\frac{\mu_{turb}}{\sigma_\kappa}\right)\frac{\partial\kappa}{\partial y}\right] \tag{4}$$

and

$$\frac{\partial(\rho u\omega)}{\partial x}+\frac{\partial(\rho\upsilon\omega)}{\partial y} = A\rho S^2 - \beta_2\rho\omega^2 + \frac{\partial}{\partial x}\left[\left(\mu+\frac{\mu_{turb}}{\sigma_\omega}\right)\frac{\partial\omega}{\partial x}\right] + \frac{\partial}{\partial y}\left[\left(\mu+\frac{\mu_{turb}}{\sigma_\omega}\right)\frac{\partial\omega}{\partial y}\right] + 2(1-F_1)\rho\frac{1}{\sigma_{\omega2}\omega}\frac{\partial\kappa}{\partial x}\frac{\partial\omega}{\partial x} + 2(1-F_1)\rho\frac{1}{\sigma_{\omega2}\omega}\frac{\partial\kappa}{\partial y}\frac{\partial\omega}{\partial y} \tag{5}$$

To complete the specification of the problem, the Menter intermittency equations are

$$\frac{\partial(\rho u\gamma)}{\partial x}+\frac{\partial(\rho v\gamma)}{\partial y}=P_{\gamma,1}-E_{\gamma,1}+P_{\gamma,2}-E_{\gamma,2}+\frac{\partial}{\partial x}\left[\left(\mu+\frac{\mu_{turb}}{\sigma_\gamma}\right)\frac{\partial\gamma}{\partial x}\right]+\frac{\partial}{\partial y}\left[\left(\mu+\frac{\mu_{turb}}{\sigma_\gamma}\right)\frac{\partial\gamma}{\partial y}\right] \quad (6)$$

and

$$\frac{\partial(\rho u\Pi)}{\partial x}+\frac{\partial(\rho v\Pi)}{\partial y}=P_{\Pi,t}+\frac{\partial}{\partial x}\left[\sigma_{\Pi,t}(\mu+\mu_{turb})\frac{\partial\Pi}{\partial x}\right]+\frac{\partial}{\partial y}\left[\sigma_{\Pi,t}(\mu+\mu_{turb})\frac{\partial\Pi}{\partial y}\right] \quad (7)$$

For a detailed discussion of these equations, the reader is referred to [22–25].

### 2.2. Numerical implementation

Simultaneous solution of the seven governing differential equations were obtained by utilizing the CFX 11.0 finite-volume-based software. The domain was chosen to extend from the channel inlet to a location 600$H$ downstream and to span the channel half height. The selection of channel length was made to ensure that the various transitions that occurred along the length of the channel were not limited by the streamwise length of the solution domain. For the discretization of the solution domain, 370,000 nodes were employed with 330,000 elements. The nodes were deployed to fulfill the requirement that the nearest-wall node location obeyed the criterion $y^+ < 1$ for all of the investigated Reynolds numbers and streamwise locations. This criterion ensures proper resolution of the critical near-wall phenomena. Graduation of the nodal distribution took account of regions of high gradients away from the wall.

All told, three parameters were varied during the course of the investigation. The first two of these have already been mentioned, namely, the shape of the velocity profile at the inlet and the turbulence intensity. The third parameter is the Reynolds number based on the hydraulic diameter (=2$H$) and the mean velocity $U$. The Reynolds number was varied over the range from 500 to 100,000.

### 2.3. Computational details

Boundary conditions at the inlet of the channel require special consideration because of the uniqueness of some of the quantities that require specification. The value of the turbulence intensity $Tu$ is sufficient to specify $\kappa$, $\omega$, and $\Pi$. Furthermore, although the inlet intermittency $\gamma$ is set equal to 1 as a default value, it immediately drops to its natural value as dictated by the flow. The inlet axial velocity profile was either uniform or of parabolic shape. These profiles are to be regarded as limiting cases. Assignment of the average inlet velocity is equivalent to prescribing the Reynolds number. The other velocity components at the inlet are zero.

At the downstream end of the solution domain, the streamwise second derivatives of all the dependent variables are zero, except for the pressure, for which a specified, area-averaged value is prescribed. At all walls, no-slip and impermeability conditions are enforced. Also, the turbulence kinetic energy and the specific dissipation rate as well as the normal derivatives of both $\gamma$ and $\Pi$ are set to zero.

The CFX 11.0 solver utilizes a false-transient, time-stepping approach whose steady-state solution is the solution of the governing equations of the problem [26]. While the fully implicit, backward-Euler, time-stepping algorithm has first-order accuracy in time, its use does not affect the accuracy of the final converged solution.

Velocity–pressure coupling was achieved on a non-staggered, collocated grid using the techniques developed by Rhie and Chow [27] and Majumdar [28]. Pressure-smoothing terms in the continuity equation suppress oscillations which can occur when both the velocity and pressure are evaluated at coincident locations.

The advection terms in the momentum equations are taken from the upwind values of the momentum flux, supplemented with an advection-correction term. The correction term reduces numerical false diffusion and is of second-order accuracy. Details of the advection treatment can be found in [29].

## 3. Results and discussion

The results to be extracted from the numerical solutions are intended both to provide information of immediate practical utility and to elucidate the fundamental physical processes governing the various transition processes that occur as the flow develops along the length of the channel.

To assist in a clear representation of the various cases under consideration, it is useful to set forth the following definitions:

### 3.1. Fully developed friction factors

Fully developed friction factors corresponding to the cases identified in Table 1 are exhibited in Fig. 1. The figure contains information which encompasses the results of the present investigation and reference lines which correspond to standard representations from the literature. The results include the friction factor response of each of the investigated cases of Table 1 to variations in the Reynolds number. Among the reference lines, that labeled 96 $Re^{-1}$ corresponds to laminar flow in a parallel-plate channel. A second reference line labeled 0.507 $Re^{-0.3}$ is an experimental correlation for low-Reynolds-number turbulent flows [11]. This reference line mates perfectly with the well-known Colebrook equation, labeled as $[1.8\log(Re/6.9)]^{-2}$, which is believed to be the best fit for turbulent friction factor data over a very wide range of Reynolds numbers [30].

An overview of Fig. 1 indicates that Case C displays a behavior which is similar to that displayed on traditional plots of friction factor versus Reynolds number. Specifically, the friction-factor results for that case coincide with those for laminar flow up to a Reynolds number of approximately 3000 and subsequently bridge smoothly across a transition region which terminates in a merging with the turbulent flow correlations at a Reynolds number of approximately 8000. This breakdown Reynolds number is in good accord with experimental data reviewed in the Introduction.

On the other hand, the results for Cases A, B, and D display a rather different behavior. For those cases, the friction-factor results are nearly coincident with those for laminar flow up to Reynolds numbers of 8000–10,000, at which point they break sharply upward and mate with the turbulent results, apparently without an extended transition regime.

It is believed that the mode of laminar breakdown for Cases A, B, and D is different from that of Case C. For the former, the breakdown is due to the instability of a fully developed profile to fluctuations inherent in the prescribed turbulence intensity. Cases B and

**Table 1**
Identification of the various cases under consideration.

| Case | Inlet velocity profile | Inlet turbulence intensity (%) |
|---|---|---|
| A | Flat | 1 |
| B | Parabolic | 1 |
| C | Flat | 5 |
| D | Parabolic | 5 |

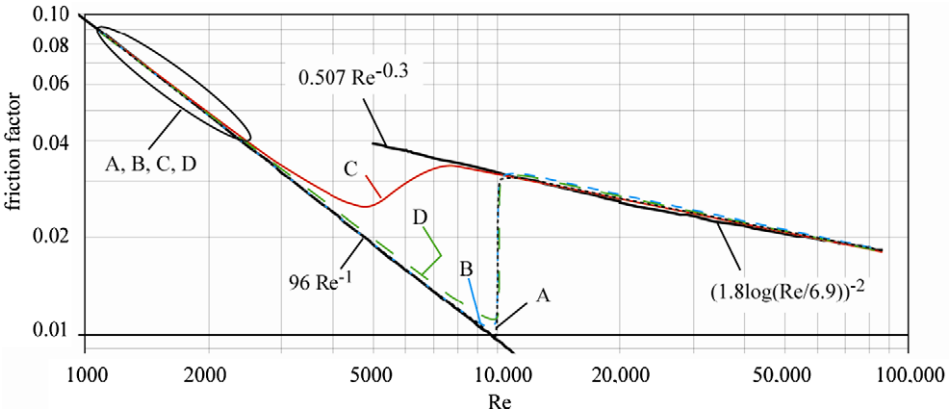


**Fig. 1.** Fully developed friction factors.

D have imposed parabolic velocity profiles at the inlet,; Case A achieves a nearly parabolic profile as the flow develops in the streamwise direction. In contrast, the behavior of the friction factors for Case C is similar to that which occurs in a boundary-layer flow.

### *3.2. Locations of laminar breakdown and attainment of the fully developed regime*

It is of considerable practical interest, especially for heat transfer applications, to know the locations at which laminar flow breaks down and where the fully developed regime begins. This information is conveyed in Figs. 2–5, which correspond respectively to Cases A-D. Attention will first be directed to Fig. 2, which pertains to a situation with a flat inlet velocity profile and a turbulence intensity of 1%. In Fig. 2, the dimensionless axial distances downstream of the inlet at which breakdown and full development occur are plotted as functions of the Reynolds number. In view of the low inlet turbulence intensity, it is reasonable to expect that laminar flow will persist to larger downstream distances than would respectively occur in practical applications where turbulence levels may be higher. This expectation is substantiated by the results of Fig. 2. In this regard, note that the lowest Reynolds number that appears in the figure is approximately 10,000, which corresponds to the breakdown of laminar flow as indicated in Fig. 1.


**Fig. 2.** Locations of laminar breakdown and full development for an initially flat velocity profile and an inlet turbulence intensity of 1%.

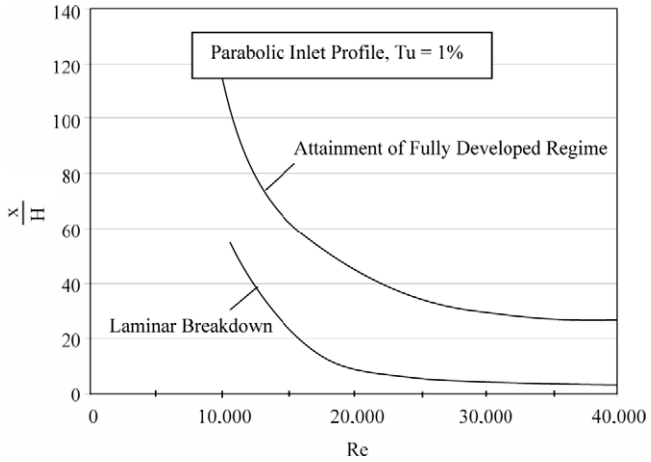


**Fig. 3.** Locations of laminar breakdown and full development for an initially parabolic velocity profile and an inlet turbulence intensity of 1%.

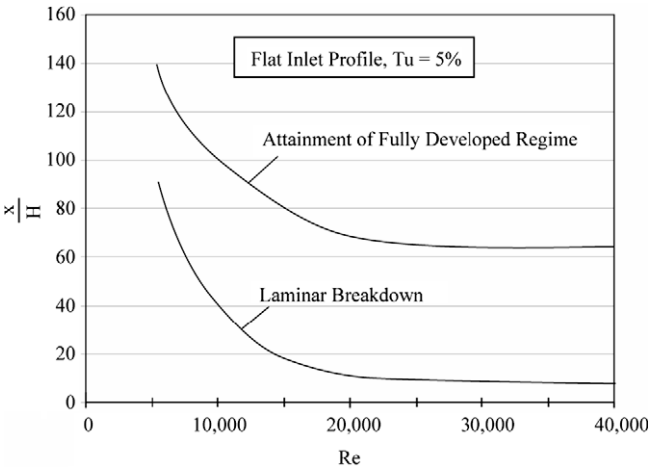


**Fig. 4.** Locations of laminar breakdown and full development for an initially flat velocity profile and an inlet turbulence intensity of 5%.

Further inspection of Fig. 2 shows that for Reynolds numbers in the range of 10,000–20,000, laminar flow persists to locations that are hundreds of channel heights downstream of the inlet. With increasing Reynolds numbers, this distance decreases markedly, but even at $Re = 50{,}000$, the length of the laminar inlet region is $100H$. With regard to the attainment of the fully developed regime,

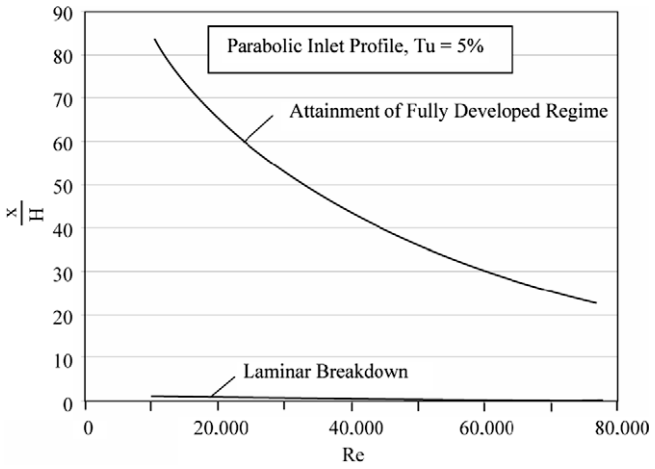


**Fig. 5.** Locations of laminar breakdown and full development for an initially parabolic velocity profile and an inlet turbulence intensity of 5%.

it is seen that, in general, it occurs approximately 50*H* downstream of the location of the breakdown of laminar flow.

Attention is now directed to Fig. 3, which pertains to a parabolic inlet velocity profile and an inlet turbulence intensity of 1%. In a certain sense, there is an incompatibility between a fully developed laminar profile and an existing turbulence intensity, albeit small. A comparison of Figs. 2 and 3 reveals a remarkable difference in the relative behaviors of these two cases. In particular, the deployment of an initially parabolic velocity profile brings about a rapid breakdown of the laminar flow. Specifically, for Reynolds numbers of ~10,000, laminar flow is seen to break down at approximately 50*H* from the inlet in the presence of a parabolic velocity profile while, as noted earlier, the flow may remain laminar for several hundred channel heights when the inlet profile is flat! Another contrast is the distance between the breakdown of laminar flow and the onset of the fully developed regime. For the conditions of Fig. 3, that distance is approximately 30*H*, whereas about 50*H* was required for Case A.

Next, results for Case C are presented in Fig. 4. It is appropriate to compare these results which pertain to an initial turbulence level of 5% with those for an inlet level of 1% as have been displayed in Fig. 2. It is clear that breakdown of laminar flow occurs at shorter downstream distances at the higher turbulence intensity, an outcome which is consistent with intuitive expectations. On the other hand, the distance between the location of laminar breakdown and that for the onset of fully developed conditions is approximately the same for the two cases.

The last case to be considered from the standpoint of locations of laminar breakdown and attainment of full development is that for an initially parabolic velocity profile and a turbulence level of 5%. While, these conditions are hardly physically compatible, they are shown as a limiting case. The results for this case, displayed in Fig. 5, are noteworthy from the standpoint of the immediacy of laminar breakdown. This outcome is surely a consequence of the high-turbulence level. The onset of the fully developed regime is also more rapidly attained.

### 3.3. Axial development of the $u_{max}/U$ ratio

A metric which reveals the nature of the fluid flow (laminar, transitional, or turbulent) is the ratio $u_{max}/U$ of the maximum to the mean velocity. In this regard, it is worthwhile to note that for fully developed laminar flow in a parallel plate channel, $u_{max}/U = 1.5$, while for turbulent flow, the value of the ratio depends on the Reynolds number. Whereas there is a reliable equation for the estimation of $u_{max}/U$ for fully turbulent flow in round pipes [31], there is no counterpart information for parallel-plate channels known to the authors. However, guidance for the values of the ratio for parallel-plate channels can be obtained by calculating the round-pipe ratio which serves as an upper bound for the channel ratio. For example, for $Re = 20{,}000$, $u_{max}/U = 1.22$ for the round pipe, and therefore, it can be expected that the ratio will be less than 1.22 for the channel flow at the same Reynolds number.

The results for $u_{max}/U$ for the four physical situations considered here are conveyed in Figs. 6–9. In these figures, $u_{max}/U$ is plotted as a function of the dimensionless axial distance for a number of representative Reynolds numbers. In Fig. 6, which corresponds to Case A (flat velocity profile and 1% turbulence intensity), the Reynolds number range extends from 6250 to 35,000. All of the $u_{max}/U$ curves begin at a value of 1, reflecting the initial flatness of the velocity profile. The velocity-development patterns naturally subdivide themselves into two categories. The first of these is a grouping in which the flow is laminar throughout, as witnessed by the monotonic approach of the velocity ratio to the laminar fully developed value of 1.5. The second category displays a transitional behavior consistent with their initial Reynolds numbers which exceed 10,000. It can be seen that there is an initial period of laminar

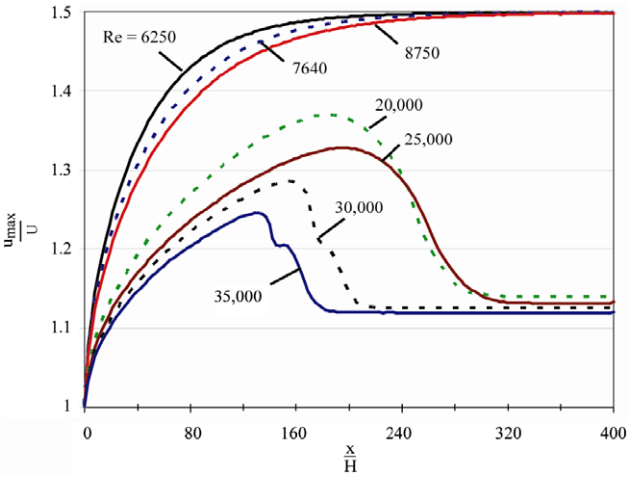


**Fig. 6.** Streamwise variation of the $u_{max}/U$ *ratio* for a flat inlet velocity profile and an inlet turbulence intensity of 1%.

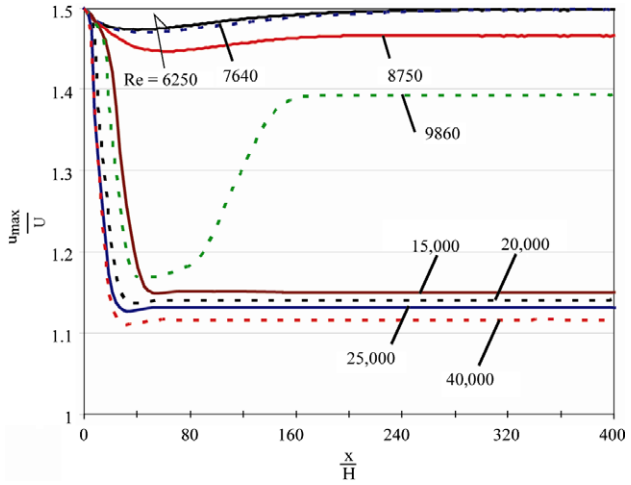


**Fig. 7.** Streamwise variation of $u_{max}/U$ for a parabolic inlet velocity profile and an inlet turbulence intensity of 1%.

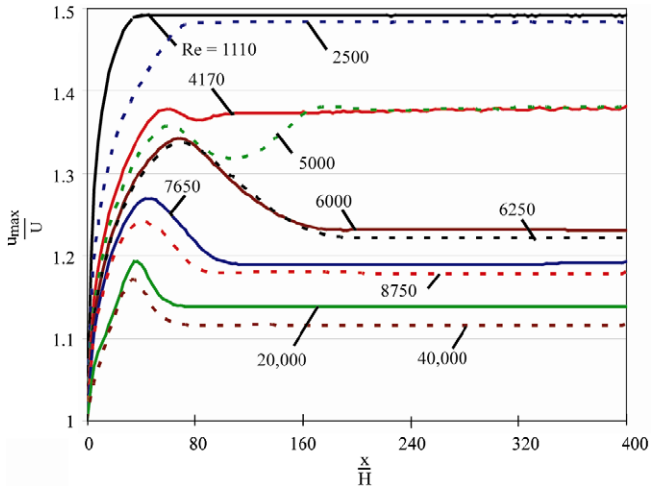


**Fig. 8.** Streamwise variation of $u_{max}/U$ for a flat inlet velocity profile and an inlet turbulence intensity of 5%.

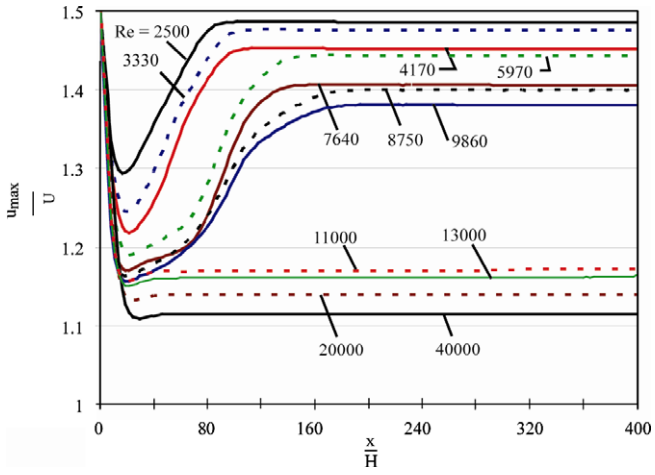


**Fig. 9.** Streamwise variation of $u_{max}/U$ for a parabolic inlet velocity profile and an inlet turbulence intensity of 5%.

development as witnessed by the fact that in all cases, $u_{max}/U$ attains values that exceed the fully developed value of approximately 1.15. The extent of the laminar development region decreases with increasing Reynolds number. Of particular interest is the local minimum in the curve for $Re = 35{,}000$. This behavior can be attributed to the opposing effects of momentum decrease and wall-friction increase.

The $u_{max}/U$ results displayed in Fig. 7 clearly differs from that of the preceding figure. First, the value of $u_{max}/U$ at the inlet reflects the fully developed nature of the profile at that location. Inspection of the figure reveals that there are three groupings of the results. The uppermost grouping encompass Reynolds numbers of 6250 and 7640. In this case, there is clear evidence that the initially parabolic profile is modified with increasing downstream distance by virtue of the presence of the initial non-zero turbulence intensity. As the turbulence intensity subsides, the parabolic shape is restored and the flow can be regarded as fully developed and laminar.

In the second category, $Re = 8750$ and 9860, the curves demonstrate an initial behavior similar to that described in the foregoing. However, owing to their higher Reynolds numbers, the turbulence intensity is not totally destroyed, so that when fully developed conditions are obtained, the flow regime is intermittent, neither fully laminar nor fully turbulent. This newly identified regime may be denoted as *fully developed intermittent*.

In the third category is a set of results for still higher Reynolds numbers. In these cases, the fully developed regime is fully turbulent. It is noteworthy that $u_{max}/U$ decreases with increasing Reynolds number in the fully developed regime. This behavior is totally consistent with the flattening of the velocity profile as the Reynolds number increases.

In the next figure, Fig. 8, results for $u_{max}/U$ are presented for the case of an initially flat velocity profile and a turbulence intensity of 5%. It can be seen from the figure that there are three identifiable behaviors. For the lowest of the Reynolds numbers, the flow develops monotonically and attains a fully developed laminar profile. In the intermediate range of Reynolds numbers (4170–8750), there is an initial laminar development which gives way to a fully developed intermittent regime. Finally, for higher Reynolds numbers, the initial laminar development eventually terminates in a fully developed turbulent flow.

The final figure in this sequence, Fig. 9, corresponds to an initial parabolic velocity profile and a turbulence level of 5%. These conditions are realistically incompatible, with the result that there is an immediate readjustment which is reflected in the sharp drop off in $u_{max}/U$. Subsequently, the readjusted profile undergoes a natural development. This natural development terminates in a fully developed intermittent flow for the lower Reynolds numbers (<10,000) and in a fully developed turbulent flow for the higher Reynolds numbers (>11,000).

## 4. Concluding remarks

This research has elucidated the process of flow development in a parallel-plate channel, taking account of the fundamental processes which govern the transitions between laminar, intermittent, and turbulent flows. It is demonstrated for several investigated cases that the conditions at the inlet of the channel play a decisive role. The inlet conditions considered here consist of profile shapes that are either flat or parabolic and turbulence intensities ($Tu$) of 1% and 5%. With regard to the profile shapes, neither is precisely achieved in practice; however, they represent limiting cases which bound the majority of realistic inlet flows. Similarly, the 1% and 5% turbulence levels are regarded as significant limiting cases, the lower of which can be achieved in the laboratory with special care and the upper may be encountered in actual operation.

The model on which the investigation is based consists of a group of seven coupled equations which express mass conservation, momentum conservation (RANS), shear–stress turbulence transport (SST), and an adapted version of the Mentor intermittency model. The version of the Mentor intermittency model was taken from the authors' adaptation which was originally tailored to flow in a circular pipe. That tailored form was successfully employed here without modification.

The friction-factor results obtained here display a variety of behaviors depending on the specified inlet conditions. For the case of a flat velocity profile at inlet and a 5% turbulence intensity, the variation in the friction factor with the Reynolds number is reminiscent of that displayed in standard textbooks. On the other hand, for the other cases (flat initial profile, $Tu = 1\%$; parabolic initial profile, $Tu = 1\%$ and 5%), the friction factor-Reynolds number relationship reveals delayed breakdown of laminar flow such that turbulence is not encountered until $Re \sim 10{,}000$.

The patterns of flow development along the length of the channel also are governed by the inlet conditions and by the value of the Reynolds number. In particular, three different fully developed regimes are identified. In addition to the well-established laminar and turbulent regimes, a new flow regime termed *fully developed intermittent*, is the natural outcome of flow development for higher

inlet turbulence intensity levels. In fact, even for the lower of the turbulence intensities considered (1%), the fully developed intermittent regime was encountered for certain Reynolds numbers for the case of a flat inlet velocity profile.

For the most realistic of the four cases considered (flat velocity profile and $Tu = 5\%$), the type of fully developed regime varied as a continuous function of the Reynolds number from laminar, to intermittent, to fully turbulent.

## References


[1] F.M. White, personal communication, June 26, 2008.
[2] M.A. Karnitz, M.C. Potter, M.C. Smith, An experimental investigation of transition of a plane Poiseuille flow, J. Fluids Eng. 96 (1974) 384–388.
[3] O.C. Jones, An improvement in the calculation of turbulent friction in rectangular ducts, J. Fluids Eng. 98 (1976) 173–181.
[4] S.J. Davies, C.M. White, An experimental study of the flow of water in pipes of rectangular section, Proc. Roy. Soc. 119 (1928) 92–107.
[5] L. Washington, W.M. Marks, Heat transfer and pressure drop in rectangular air passages, Ind. Eng. Chem. 29 (1937) 337–345.
[6] J.E. Walker, G.A. Whan, R.R. Rothfus, Fluid friction in noncircular ducts, AIChE J. 3 (1957) 484–489.
[7] G.A. Whan, R.R. Rothfus, Characteristics of transition flow between parallel plates, AIChE J. 5 (1959) 204–208.
[8] R.W. Hanks, H.-C. Ruo, Laminar-turbulent transition in ducts of rectangular cross section, Ind. Eng. Chem. Fund. 5 (1966) 558–561.
[9] V.C. Patel, M.R. Head, Some observations on skin friction and velocity profiles in fully developed pipe and channel flows, J. Fluid Mech. 38 (1969) 181–201.
[10] G.S. Beavers, E.M. Sparrow, R.A. Magnuson, Experiments on the breakdown of laminar flow in a parallel-plate channel, Int. J. Heat Mass Transfer 13 (1970) 809–815.
[11] G.S. Beavers, E.M. Sparrow, J. Lloyd, Low Reynolds number turbulent flow in large aspect ratio rectangular ducts, J. Basic Eng. 93 (1971) 296–299.
[12] S.A. Orszag, Accurate solution of the Orr–Somerfeld stability equation, J. Fluid Mech. 50 (1971) 689–703.
[13] S.A. Orszag, L.C. Kells, Transition to turbulence in plane Poiseuille and plane Couette flow, J. Fluid Mech. 96 (1980) 159–205.
[14] T.A. Zang, S.E. Krist, Numerical experiments on stability and transition in plane channel flow, Theor. Comp. Fluid Dyn. 1 (1989) 41–64.
[15] J. Jimenez, Transition to turbulence in two-dimensional Poiseuille flow, J. Fluid Mech. 218 (1990) 265–297.
[16] T. Tatsumi, T. Yoshimura, Stability of the laminar flow in a rectangular duct, J. Fluid Mech. 212 (1990) 437–449.
[17] D.S. Henningson, J. Kim, On turbulent spots in plane Poiseuille flow, J. Fluid Mech. 228 (1991) 183–205.
[18] M. Nishioka, S. Iida, Y. Ichikawa, An experimental Investigation of the stability of plane Poiseuille flow, J. Fluid Mech. 72 (1975) 731–751.
[19] D.R. Carlson, S.E. Widnall, M.F. Peeters, A flow-visualization study of transition in plane Poiseuille flow, J. Fluid Mech. 121 (1982) 487–505.
[20] F. Alavyoon, D.S. Henningson, P.H. Alfredsson, Turbulent spots in plane Poiseuille flow–flow visualization, Phys. Fluids 29 (1986) 1328–1331.
[21] J.P. Abraham, J.C.K. Tong, E.M. Sparrow, Numerical simulation of laminar-to-turbulent transition and intermittent internal flows, Num. Heat Transfer 54 (2008) 103–115.
[22] F.R. Menter, T. Esch, S. Kubacki, Transition modelling based on local variables, in: 5th International Symposium on Engineering Turbulence Modeling and Measurements, Mallorca, Spain, 2002.
[23] F.R. Menter, R.B. Langtry, S.R. Likki, Y.B. Suzen. P.G. Huang, S.Volker, A correlation-based transition model using local variables. Part I – Model formulation, in: Proceedings of ASME Turbo Expo Power for Land, Sea, and Air, Vienna, Austria, June 14–17, 2004.
[24] F.R. Menter, R.B. Langtry, S.R. Likki, Y.B. Suzen. P.G. Huang, S.Volker, A Correlation-based transition model using local variables. Part II – Test cases and industrial applications, in: Proceedings of ASME Turbo Expo Power for Land, Sea, and Air, Vienna, Austria, June 14–17, 2004.
[25] J. Abraham, E. Sparrow, J. Tong, Heat transfer in all pipe flow regimes – laminar, transitional/intermittent, and turbulent, Int. J. Heat Mass Transfer 52 (2009) 557–563.
[26] CFX Version 11.0 Manual, ANSYS, Inc, Canonsburg, PA.
[27] C.M. Rhie, W.L. Chow, A Numerical Study of the Turbulent Flow Past an Isolated Airfoil with Trailing Edge Separation, AIAA paper No. 82-0998, 1982.
[28] S.R. Majumdar, Role of underrelaxation in momentum interpolation for calculation of flow with nonstaggered grids, Num. Heat Transfer 13 (1988) 125–132.
[29] T.J. Barth, D.C. Jesperson, The Design and Applications of Upwind Schemes on Unstructured Meshes, AIAA paper No. 89-03, 1989.
[30] C.F. Colebrook, Turbulent flow in pipes with particular reference to the transition between smooth and rough pipe laws, J. Inst. Civ. Eng. Lond. 11 (1938) 133–156.
[31] F.M. White, Fluid Mechanics, sixth ed., McGraw-Hill, Boston, 2008. p. 361.